American Mineralogist, Volume 87, pages 1113–1120, 2002

Intersite distribution of Fe^{2+} and Mg in the spinel (sensu stricto)–hercynite series by single-crystal X-ray diffraction

GIOVANNI B. ANDREOZZI* AND SERGIO LUCCHESI†

Dipartimento di Scienze della Terra, Università di Roma "La Sapienza", P.le A. Moro 5, 00185 Roma, Italy

ABSTRACT

The influence of composition on Fe^{2+}-Mg intracrystalline distribution was studied in eleven synthetic crystals belonging to the spinel (sensu stricto)–hercynite series $(Mg_{1-y}Fe^{2+}_y)Al_2O_4$, with $0 \le y \le 1$, produced by flux-growth at 800 °C. Samples were analyzed by single-crystal X-ray diffraction and electron microprobe methods, and found to be chemically homogeneous with only minor Fe^{3+}, which substitutes for Al and increases up to 0.09 atoms per formula unit with total Fe. Structural parameters *a*, *u*, T-O, and M-O increase with hercynite content and, among bond distances, T-O shows the maximum change, from 1.920 to 1.968 Å. The *a* variation from 8.0855 to 8.1646 Å is essentially caused by the T-O increase that, in turn, is due to the cooperative effects of (1) $Fe^{2+} \rightarrow Mg$ substitution and (2) decrease of inversion from 0.23 to 0.15 along the series.

Intracrystalline cation distribution was obtained by a minimization procedure that takes into account structural and chemical data. The T site is mainly populated by Mg and Fe^{2+} but, at a given temperature, Fe^{2+} shows a marked preference for tetrahedral coordination with respect to Mg. The influence of composition and temperature on Fe-Mg intracrystalline distribution was modeled within the framework of the general thermodynamic model of O'Neill and Navrotsky for spinel binary solid solutions. The inversion values observed in our samples agree very well with those calculated by the model. Both measured and calculated amounts of octahedral Fe^{2+} ($^{VI}Fe^{2+}$) show a non-linear increase from spinel s.s. to hercynite. Consequently, the $^{VI}Fe^{2+}/Fe^{2+}_{tot.}$ ratio is not constant along the join, but increases from zero to 15% toward the hercynite end-member. This behavior explains the very limited Fe^{2+} inversion observed in natural spinels, which usually belong to the hercynite-poor part of the join.

INTRODUCTION

Spinels have a very compact oxygen array, with cations in tetrahedral (T) and octahedral (M) coordination. They may be described by the $^{IV}(A_{1-i}B_i)^{VI}(B_{2-i}A_i)O_4$ structural formula, in which IV and VI represent tetrahedrally and octahedrally coordinated sites, A and B cations with variable valence distributed in T and M sites, and *i* the inversion parameter. Normal spinels show $i \cong 0$ (e.g., $MgAl_2O_4$, $FeAl_2O_4$); inverse ones have $i \cong 1$ (e.g., $MgFe_2O_4$, $FeFe_2O_4$). Symmetry is cubic ($Fd\bar{3}m$), with the single oxygen atom at *u*, *u*, *u* fractional coordinates; T and M sites have fixed positions. Modifications of T-O and M-O bond distances to accommodate various chemical compositions and/or cation ordering determine variations in the oxygen positional parameter *u* and the cell edge *a* (Hafner 1960; Hill et al. 1979).

Within the spinel group, minerals of the $(Mg,Fe^{2+})(Al,Fe^{3+})_2O_4$ system are widespread in most geological environments. A complete solid solution exists between spinel sensu stricto (s.s.), $MgAl_2O_4$, and hercynite, $FeAl_2O_4$, whereas a large immiscibility gap is observed between hercynite and Mg-Fe^{2+}-ferrites (Turnock and Eugster 1962; Lehmann and Roux 1986). As a consequence, most natural crystals belong to the spinel s.s.-hercynite series with a minor ferrite component. This is the case, for example, for spinels from volcanic xenoliths (Lucchesi and Della Giusta 1997; Lucchesi et al. 1998a), websteritic dykes in a peridotite (Basso et al. 1984), and metamorphosed limestones (Carbonin et al. 1996).

In spinels, intracrystalline cation distribution depends on temperature and has been proposed as a potential geothermometer (Della Giusta et al. 1996; Harrison et al. 1998; Princivalle et al. 1999; Andreozzi et al. 2000). However, the influence of bulk composition on intracrystalline cation distribution has been pointed out as a crucial factor (O'Neill and Navrotsky 1983, 1984; Waerenborgh et al. 1994a, 1994b; Andreozzi et al. 2001). Both spinel s.s. and hercynite end-members are characterized by a nearly normal configuration, with progressive increase of inversion with increasing equilibration temperature (e.g., Roth 1964; Hill 1984; Bohlen et al. 1986; Harrison et al. 1998; Redfern et al. 1999; Andreozzi et al. 2000). The crystal chemistry of the hercynite end-member is complicated because of frequent deviations from stoichiometry due to Fe^{3+} and cation vacancies (Slack 1964; Cremer 1969; Mason and Bowen 1981). The substitution of Fe^{3+} for Fe^{2+} and the presence of cation vacancies were claimed by Waerenborgh et al. (1994a) to be determinant in producing the discrepancy between their experimental data and those calculated using the O'Neill and Navrotsky (1984) model. Moreover, they suggested that the value of site preference enthalpy α_{Fe-Al}, estimated by O'Neill

* E-mail: gianni.andreozzi@uniroma1.it
† sergio.lucchesi@uniroma1.it

and Navrotsky to be about 52 kJ/mol, had to approach 35 kJ/mol. Actually, an experimental value of α_{Fe-Al} = 31.3 kJ/mol was later obtained by Harrison et al. (1998) on synthetic $FeAl_2O_4$. However, calculations with the new α-value still could not account for the large disagreement observed between experimental and calculated inversion data. This disagreement could be explained not only by vacancies, as the authors claimed, but also by some underestimation of $^{VI}Fe^{2+}$ content, due to difficulties in accurately determining Fe^{2+} distribution by Mössbauer spectroscopy.

In $FeAl_2O_4$, a detailed study of Fe^{2+}-Al disordering with temperature was carried out by Larsson et al. (1994) using powder X-ray diffraction (XRD) and Mössbauer spectroscopy, and by Harrison et al. (1998) using in situ neutron diffraction, and both studies revealed Fe^{2+} inversion up to 0.22 at 1150 °C. In $MgAl_2O_4$, higher inversion values, up to 0.30 at 1100 °C, were observed (Andreozzi et al. 2000, and references therein). This finding suggests that, compared with Fe^{2+}, Mg has some preference in substituting for octahedral Al. Hence, a compositional influence on cation distribution is to be expected along the spinel s.s.-hercynite join. However, published results on intermediate compositions are not only scarce but also controversial: Nozik and Kocharov (1989) measured zero $^{VI}Fe^{2+}$ content in a synthetic intermediate sample, whereas Larsson (1994, 1995), who studied both natural and synthetic samples, retrieved a constant $^{VI}Fe^{2+}/Fe^{2+}_{tot.}$ ratio of about 20%, indicating that Fe^{2+} ordering is almost unaffected by hercynite content.

Due to such contradictory results in the literature, the influence of composition on intracrystalline cation distribution deserves further investigation and needs to be verified on a homogeneous set of samples representative of the whole spinel s.s.–hercynite series. Because the study of natural samples is rather difficult, due to the ubiquitous presence of minor elements and the rarity of compositions close to the end-members, synthetic single crystals were produced in the system $(Mg_{1-y}Fe^{2+}_y)Al_2O_4$ ($0 \le y \le 1$). Their crystal chemistry was studied by single-crystal XRD and electron microprobe analysis: both cation distributions and induced structural modifications are covered with in the present paper. Mössbauer and optical absorption spectra were collected on the same materials and are discussed separately (Hålenius et al. 2002).

Experimental procedures

Crystal synthesis

Single crystals along the spinel s.s.-hercynite join were synthesized using a flux-growth method (Andreozzi 1999). Analytical grade $Al(OH)_3$, MgO, and Fe_2O_3 powders were dried and dehydrated at 1000 °C for 12 h before mixing with $Na_2B_4O_7$, used as the flux compound. About 5 g of the starting material was thoroughly ground under acetone in an agate mortar and mixed, at flux/reagents ratios ranging from 1.3 to 1.4. A 10 cc crucible of yttria-stabilized Pt/Au(5%) was employed, due to its good resistance to chemicals at high temperatures in reducing conditions (Okaj et al. 1996).

Thermal runs were performed in a vertical furnace equipped with Tylan CO_2:H_2 flow controllers. Continuous flow of the two gases in the ratio 2:1 was adopted to obtain an oxygen fugacity ranging from 10^{-11} to 10^{-17} bars when the temperature was varied from 1200 to 900 °C. The f_{O_2} values were within –0.3 to +1.2 log units relative to the iron-wüstite solid buffer. To obtain a homogeneous melt, the flux-reagents mix was heated for 24 hours at 1200 °C, and then the temperature was decreased by slow cooling (2–4 °C/h). Turning off the furnace ended thermal runs, and the product was cooled down to room temperature. Products consisted of spinel single crystals, a B-rich glass, and sporadic borate crystals. The sodium borate glass was dissolved in warm, dilute HCl solution, reducing final products to euhedral or subhedral spinel octahedra (range 0.1–1.0 mm across). Up to 200 mg of high-quality spinel crystals, about 0.2–0.5 mm across, were recovered from each experiment.

The resultant crystals varied in color depending on hercynite content: from colorless (spinel s.s.) to deep green or black (hercynite). Crystals from most runs proved to be optically and chemically homogeneous. Only the most Fe-rich sample (He100c) showed a thin, light-colored rim, and in this case the crystals were crushed and their cores selected for X-ray study. For every composition, some crystals were selected for the present study, while other material was used for Mössbauer and single-crystal optical absorption spectroscopy (Hålenius et al. 2002).

X-ray diffraction and structural analysis

Small equidimensional fragments of the crystals were selected, cemented on a glass capillary, and mounted on a Siemens P4 four-circle, single-crystal automated diffractometer for X-ray data collection (Table 1). Unit-cell parameters (Table 2) were obtained after centering 12 independent reflections and their Friedel pairs chosen in the $83° < 2\theta < 92°$ range on both sides of the direct beam, with Mo$K\alpha_1$ radiation (λ = 0.70930 Å). For collection of diffraction intensity data, one-eighth of the reciprocal space was examined with the ω scan method and fixed scan range, using Mo$K\alpha$ radiation (λ = 0.71073 Å). Scan speed was variable, depending on reflection intensity, estimated with a pre-scan. Background was measured with a stationary counter and crystal at the beginning and end of each scan, in both cases for half the scan time. Three standard reflections were monitored every 47 measurements. Further details of the experimental conditions may be found in Lucchesi et al. (1997).

The SHELXTL-PC program package allowed reduction of X-ray diffraction data. Intensities were corrected for polarization and Lorentz effects. An absorption correction was made with a semi-empirical method, using intensities from the ψ-scans of 13 non-equivalent reflections collected in the range 10–90° 2θ. Reflections with $I > 2\sigma(I)$ were considered as observed, and the original set of about 624 data was reduced to 147–149 independent reflections. No significant deviations from $Fd\bar{3}m$ symmetry were noted: the appearance of forbidden space-group reflections such as 200 was attributed, on the basis of ψ-scan checks, to double reflection (Tokonami and Horiuchi 1980). During structural refinement, variable parameters were: scale factor, oxygen coordinate, mean atomic numbers (m.a.n.) of the T and M sites, displacement parameters, and isotropic secondary extinction coefficient (Table 2). The starting oxygen coordinate was that proposed by Princivalle et al. (1989), the origin being set at $\bar{3}m$. No chemical constraints

were applied during refinement. Fully ionized scattering curves for all elements were used, as they furnished the best values of conventional agreement factors over all $\sin\theta/\lambda$ intervals and the best coherence between measured and calculated F(222), the latter structural factor being particularly sensitive to ionization levels of the atomic species of both M and O sites (Della Giusta et al. 1996). This combination gave satisfactory agreement between values of total m.a.n. obtained by structural refinement and electron microprobe analysis (within 1σ of the latter). Off-diagonal displacement parameters were extremely small and of the same magnitude as their uncertainties, when not forced by symmetry to zero; thus, only U_{11} are shown in Table 2. The complete set of displacement parameters is available from the authors on request. Three cycles of isotropic refinement were followed by anisotropic cycles until convergence to very satisfactory R values (Table 2).

Chemical analysis

After X-ray data collection, the same crystals were mounted on glass slides, polished, and carbon coated for electron microprobe analysis (WDS method) on a Cameca-Camebax instrument operating at an accelerating potential of 15 kV and a sample current of 15 nA. Synthetic MgO, Fe_2O_3, and Al_2O_3 were used as standards, and a synthetic $MgAl_2O_4$ sample was used as reference material. For raw data reduction, the PAP computer program was applied (Pouchou and Pichoir 1984). Each element determination (Table 3) was accepted after checking that the intensity of analyzed standards before and after each measurement was within 1.00 ± 0.01. The FeO and Fe_2O_3 contents of the crystals used for XRD were calculated on the basis of charge-balance requirements and turned out to fit Mössbauer data collected on the same material. Sodium was checked as a possible contaminant, but was not detected in any sample. The absence of B was confirmed by means of $^{11}B(p,2\alpha)^4He$ nuclear reaction analysis (Kristiansson et al. 1999).

TABLE 1. Parameters for X-ray data collection

Unit-cell parameter determination	
Radiation (Å)	Mo$K\alpha_1$ 0.70930
Reflections used	12 (Friedel pairs on both +2θ and –2θ)
Range (2θ)	83–92°
Temperature (K)	296
Diffraction intensity collection	
Radiation (Å)	Mo$K\alpha$ 0.71073
Monochromator	High crystallinity graphite crystal
Range (2θ)	3–95°
Reciprocal space range	$0 \le h,k,l \le 17$
Scan method	ω
Scan range (2θ)	Fixed, 2.4°
Scan speed (2θ/min)	Variable, 2.93–29.30°
Temperature (K)	296
Data reduction	
Refinement	SHELXTL-PC
Corrections	Lorentz, Polarization
Absorption correction	Semi-empirical, 13 Ψ scans

Cation distribution

As previously discussed, A and B cations are expected to be disordered between T and M sites. Several different procedures may be adopted to determine cation distribution, and very satisfactory results have recently been obtained by combining data from single-crystal X-ray structural refinements and electron microprobe analysis (Carbonin et al. 1996; Della Giusta et al. 1996; Lucchesi et al. 1997, 1998a, 1998b, 1999). This approach simultaneously takes into account both structural and chemical data and reproduces the observed parameters by optimizing cation distributions. Differences between measured and calculated parameters are minimized by the "chi-square" function:

$$F(X_i) = \sum_{j=1}^{n} \left\{ \left[\left(O_j - C_j(X_i) \right) / \sigma_j \right]^2 \right\} / n \qquad (1)$$

where O_j is the observed quantity, σ_j its standard deviation, X_i the variables, i.e., cation fractions in T and M sites, and $C_j(X_i)$ the same quantity as O_j calculated by means of X_i parameters. The n O_j quantities taken into account were: unit-cell and oxygen parameter, m.a.n. of T and M sites, total atomic proportions given by microprobe analyses, and constraints imposed by crystal chemistry (total charges and occupancies of T and M sites). Several minimization cycles of Equation 1 up to convergence were performed using a home-developed calculation routine. Further details about the minimization procedure may be found in Lavina et al. (2002).

M-O and T-O bond distances were calculated as the linear contribution of each cation multiplied by its specific site bond distance, the latter refined on the basis of analysis of more than

TABLE 2. Results of structure refinement of synthetic crystals belonging to spinel s.s.-hercynite series

Sample	SP3/10a	He2f/e	He3a/b	He4a/c	He4b/d	He5a/a	He6a/e	He7a/b	He8a/h	He9a/h	He100c/a
a (Å)	8.0855(2)	8.0895(3)	8.0937(3)	8.1006(3)	8.1071(3)	8.1134(3)	8.1221(3)	8.1306(3)	8.1406(3)	8.1494(4)	8.1646(3)
u	0.26213(5)	0.26218(4)	0.26215(5)	0.26258(5)	0.26278(5)	0.26280(5)	0.26308(5)	0.26306(7)	0.26362(6)	0.26377(7)	0.26416(8)
T-O (Å)	1.9204(4)	1.9221(3)	1.9227(4)	1.9303(4)	1.9347(4)	1.9365(4)	1.9425(4)	1.9471(6)	1.9545(5)	1.9588(6)	1.9679(7)
M-O (Å)	1.9283(4)	1.9289(3)	1.9301(4)	1.9286(4)	1.9287(4)	1.9301(4)	1.9301(4)	1.9309(6)	1.9307(5)	1.9317(6)	1.9325(7)
T m.a.n.	11.99(10)	12.77(7)	13.87(9)	14.87(10)	15.99(8)	17.05(10)	18.32(10)	19.71(12)	21.21(11)	22.64(18)	24.57(17)
M m.a.n.	12.82(7)	12.81(5)	12.81(5)	12.86(5)	13.00(4)	13.03(5)	13.26(5)	13.40(5)	13.67(4)	13.95(6)	14.55(7)
U_{11}T (Å^2×10^4)*	42(2)	46(2)	52(2)	57(2)	54(1)	73(2)	61(1)	76(1)	65(1)	76(1)	78(1)
U_{11}M (Å^2×10^4)*	43(2)	44(1)	41(1)	46(1)	44(1)	58(1)	44(1)	56(1)	42(1)	51(1)	50(2)
U_{11}O (Å^2×10^4)*	75(2)	79(1)	81(1)	83(1)	80(1)	98(1)	84(1)	99(1)	87(1)	97(2)	99(2)
R_{all}	3.71	1.80	2.65	1.95	1.68	1.73	1.68	2.07	1.75	2.66	2.31
No. of refl.	147	147	147	147	147	149	149	149	149	149	149

Notes: Estimated standard deviation (±1σ) in brackets; m.a.n. = mean atomic number; no. of refl. = unique reflections from set of observed ones [$I > 2\sigma(I)$].

* Off-diagonal displacement parameters are extremely small and of the same magnitude as their σ, when not forced by symmetry to zero, and thus only U_{11} are shown.

TABLE 3. Chemical composition of synthetic crystals belonging to spinel s.s.-hercynite series

Sample	SP3/10a	He2f/e	He3a/b	He4a/c	He4b/d	He5a/a	He6a/e	He7a/b	He8a/h	He9a/h	He100c/a
MgO	28.5(3)	26.6(3)	24.7(4)	22.4(6)	19.3(2)	17.0(3)	13.8(3)	10.4(2)	7.3(1)	4.2(2)	–
$FeO_{tot.}$	–	2.6(4)	5.4(1)	9.4(9)	13.7(3)	17.5(2)	22.6(5)	27.5(3)	33.0(3)	38.0(4)	44.7(2)
Al_2O_3	71.0(3)	71.0(3)	69.6(5)	68.8(6)	66.8(2)	66.3(6)	63.4(3)	62.3(4)	59.8(1)	58.0(3)	55.5(4)
Total	99.5	100.2	99.7	100.6	99.8	100.8	99.8	100.2	100.1	100.2	100.2
$FeO_{calc.}$	–	2.5(3)	5.0(4)	8.9(8)	13.0(3)	16.7(4)	20.9(4)	26.0(4)	30.4(1)	35.0(3)	40.9(2)
$Fe_2O_{3\,calc.}$	–	0.1(1)	0.4(4)	0.6(3)	0.8(3)	0.9(4)	1.9(3)	1.7(4)	2.9(3)	3.3(4)	4.2(3)
Total	99.5	100.2	99.7	100.7	99.9	100.9	100.0	100.4	100.4	100.5	100.6
Cations on the basis of 4 oxygen atoms											
Mg	1.011(6)	0.947(6)	0.895(12)	0.818(18)	0.726(6)	0.645(9)	0.541(9)	0.417(7)	0.301(3)	0.175(7)	–
Fe^{2+}	–	0.051(7)	0.102(9)	0.182(18)	0.274(6)	0.354(8)	0.459(9)	0.583(7)	0.699(3)	0.825(7)	1.000(1)
Al	1.992(4)	2.000(4)	1.994(11)	1.989(6)	1.984(5)	1.982(9)	1.963(6)	1.967(8)	1.941(6)	1.929(9)	1.908(6)
Fe^{3+}	–	0.001(2)	0.008(8)	0.011(6)	0.016(5)	0.018(8)	0.037(6)	0.033(8)	0.059(6)	0.071(9)	0.092(6)
Total	3.003	2.999	2.999	3.000	3.000	3.000	3.000	3.000	3.000	3.000	3.000
$Fe^{2+}/Fe_{tot.}$ EMP	–	0.98	0.93	0.94	0.94	0.95	0.93	0.95	0.92	0.92	0.92
$Fe^{2+}/Fe_{tot.}$ MS	–	0.98	0.96	n.a.	0.96	0.96	0.95	0.96	0.94	0.94	0.94

Notes: Average of 15 electron microprobe analyses. Estimated standard deviation (±1σ) in brackets. EMP = $Fe^{2+}/Fe_{tot.}$ ratio calculated from electron microprobe analysis. MS = $Fe^{2+}/Fe_{tot.}$ ratio measured from Mössbauer spectroscopy data (Hålenius et al. 2002); n.a. = not available.

200 spinel structural data from the literature (Lavina et al. 2002). Final $F(X_i)$ values ranging from 0.1 to 1.1 were obtained, confirming that all chemical and structural parameters were reproduced on average within ±1σ, and hence that the corresponding cation distributions are highly reliable (Table 4).

CRYSTAL CHEMISTRY OF THE SPINEL S.S.–HERCYNITE SERIES

The studied crystal fragments are chemically homogeneous and representative of the whole spinel s.s.–hercynite series, with chemical composition dominated by $Fe^{2+} \rightarrow Mg$ substitution (Table 3). All samples contain very minor Fe^{3+}, which substitutes for Al and increases up to 0.09 atoms per formula unit (apfu) with total Fe. The Fe^{2+}/Fe^{3+} ratios calculated from stoichiometry turned out to fit Mössbauer spectroscopy data collected on the same materials (Hålenius et al. 2002). The observed very minor deviations fall within the experimental uncertainty of both methods. No indications of cation vacancies with respect to AB_2O_4 stoichiometry were thus revealed by comparison of structural and chemical data.

Structural parameters *a*, *u*, T-O, and M-O increase with hercynite content (Table 2 and Fig. 1). Among bond distances, T-O shows the largest variation, from 1.920 to 1.968 Å, whereas M-O remains almost constant (from 1.928 to 1.933 Å). As a consequence, the relatively large *a* variation from 8.0855 to 8.1646 Å is essentially due to T-O increase. It is noteworthy that T-O and M-O take on the same value in sample He4a/c, which has a hercynite content of about 20%; beyond this composition T-O becomes markedly larger than M-O (Fig. 1b).

The observed structural modifications are caused by both compositional changes and intracrystalline disorder. In particular, the T site is occupied mainly by either Mg or Fe^{2+}, depending on the amount of hercynite. Minor Al is also present in this site due to inversion, but its content decreases with the hercynite component (Fig. 2a). Because relationships among cation radii are of the type $Fe^{2+} > Mg > Al$, the observed T-O increase to-

TABLE 4. Intracrystalline cation distribution and differences between observed and calculated structural parameters of synthetic crystals belonging to spinel s.s.-hercynite series

Sample	SP3/10a	He2f/e	He3a/b	He4a/c	He4b/d	He5a/a	He6a/e	He7a/b	He8a/h	He9a/h	He100c/a
T site											
Mg	0.765	0.715	0.640	0.588	0.514	0.434	0.366	0.267	0.185	0.101	–
Fe^{2+}	–	0.046	0.111	0.188	0.272	0.347	0.424	0.531	0.630	0.713	0.849
Al	0.235	0.239	0.249	0.224	0.214	0.219	0.194	0.192	0.168	0.152	0.133
Fe^{3+}	–	0.000	0.000	0.000	0.000	0.000	0.016	0.010	0.017	0.034	0.018
Total	1.000	1.000	1.000	1.000	1.000	1.000	1.000	1.000	1.000	1.000	1.000
M site											
Mg	0.235	0.239	0.250	0.227	0.213	0.215	0.178	0.153	0.118	0.076	–
Fe^{2+}	–	0.000	0.000	0.000	0.004	0.008	0.035	0.054	0.072	0.114	0.153
Al	1.765	1.761	1.750	1.766	1.769	1.762	1.768	1.772	1.770	1.774	1.765
Fe^{3+}	–	0.000	0.000	0.007	0.015	0.016	0.020	0.022	0.041	0.037	0.082
Total	2.000	2.000	2.000	2.000	2.001	2.001	2.001	2.001	2.001	2.001	2.000
$F(X_i)$	0.86	0.67	0.52	0.39	0.12	0.34	0.22	0.41	0.34	0.16	1.98
Δa (Å)	0.0000	0.0000	0.0000	0.0000	0.0000	0.0000	0.0000	0.0001	0.0001	0.0001	0.0002
Δ_{T-O} (Å)	0.0000	0.0000	0.0001	0.0002	0.0000	0.0000	0.0001	0.0001	0.0001	0.0000	0.0004
Δ_{M-O} (Å)	0.0000	0.0000	0.0001	0.0001	0.0000	0.0000	0.0000	0.0001	0.0000	0.0000	0.0003
ΔT m.a.n.	0.25	0.12	0.06	0.01	0.01	0.04	0.05	0.06	0.03	0.01	0.30
ΔM m.a.n.	0.06	0.08	0.06	0.08	0.01	0.03	0.02	0.03	0.02	0.01	0.01

Notes: $F(X_i)$ = sum of square residuals divided by number of observed parameters; Δ = absolute deviation; m.a.n. = mean atomic number. Ideal bond distances used (Å): $^{IV}Mg - O = 1.966$; $^{IV}Fe^{2+} - O = 2.000$; $^{IV}Al - O = 1.774$; $^{IV}Fe^{3+} - O = 1.875$; $^{VI}Mg - O = 2.082$; $^{VI}Fe^{2+} - O = 2.146$; $^{VI}Al - O = 1.908$; $^{VI}Fe^{3+} - O = 2.025$.

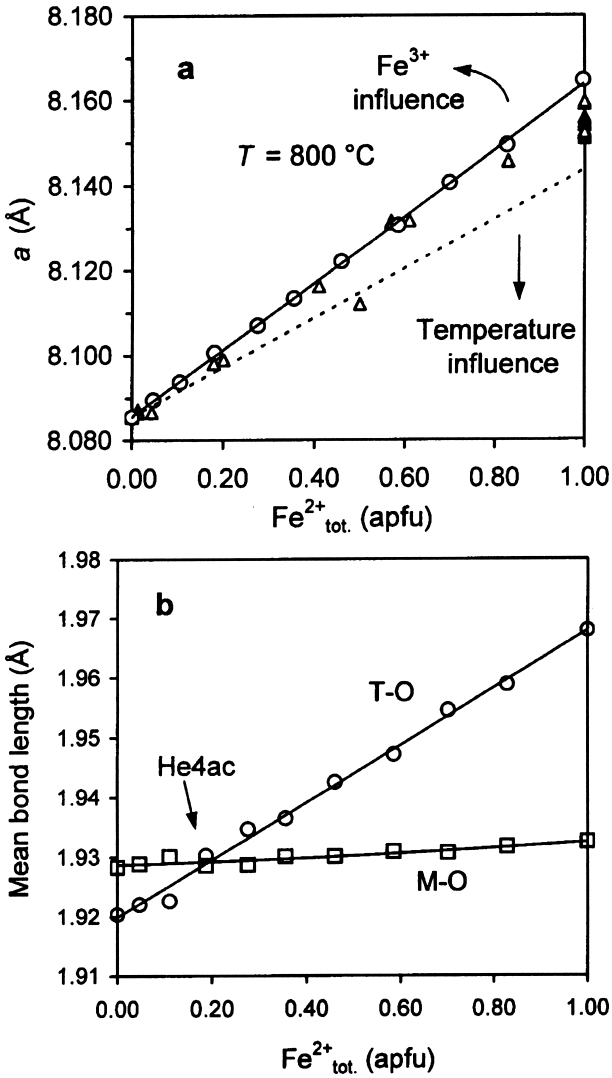

FIGURE 1. Variations in structural parameters as a function of hercynite content in spinel s.s.-hercynite crystals. (**a**) Unit-cell parameter vs. total Fe^{2+} content. Circles = data from present work, interpolated by solid line; dashed line = ideal trend calculated for $MgAl_2O_4$-$FeAl_2O_4$ join at 800 °C; triangles = data from literature; outlier is sample from Nozik and Kocharov (1989). With respect to ideal trend at 800 °C, slope increases because of Fe^{3+} content and decreases because of higher equilibration temperatures. (**b**) T-O and M-O bond distances vs. total Fe^{2+} content. Sample He4a/c shows almost equal values for T-O and M-O distances.

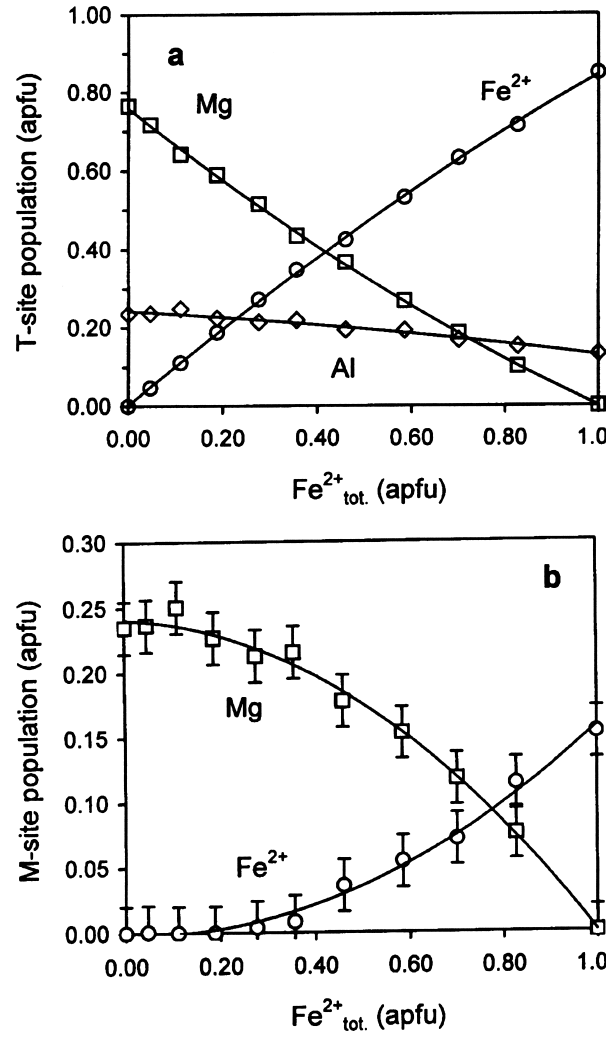

FIGURE 2. Site population of spinel s.s.-hercynite synthetic samples as a function of hercynite content: (**a**) T site; (**b**) M site. Symbol dimensions are proportional to ±2σ, except where error bars are shown.

ward hercynite is therefore due to the cooperative effects of (1) $^{IV}Fe^{2+} \rightarrow {}^{IV}Mg$ substitution and (2) decrease of inversion, i.e., ^{IV}Al content. The M-O variation, almost one order of magnitude smaller than that involving T-O, is essentially produced by the increment of $^{VI}Fe^{2+}$ (Fig. 2b), but a small contribution is also due to Fe^{3+}, which substitutes for Al and mainly populates the M site (Table 4).

Previous discussion has evidenced that, along the spinel s.s.–hercynite join, the increase in the unit-cell parameter is due to $Fe^{2+} \rightarrow Mg$ substitution, whereas for any fixed composition an increase of inversion (i.e., of equilibration temperature) determines cell contraction (Fig. 1a). At 800 °C, assuming an inversion of 0.23 and 0.15 for spinel s.s. and hercynite, respectively (Andreozzi et al. 2000; Harrison et al. 1998), the ideal trend between cell parameter and Fe^{2+} content (apfu) is described by the linear relation:

$$a = 8.0855 + 0.0583\ Fe^{2+}. \quad (2)$$

However, because of the almost ubiquitous presence of minor Fe^{3+} (which substitutes for Al in our samples and in those from the literature), this ideal trend is rarely followed. In fact, our samples plot higher than the ideal trend, the synthetic samples of Zhukovskaya et al. (1980), characterized by Fe^{3+} contents lower than ours, plot slightly below the observed trend, whereas the sample studied by Nozik and Kocharov (1989), the composition of which is close to stoichiometry, plots very close to the ideal trend (Fig. 1a).

THERMODYNAMIC MODELING OF CATION DISTRIBUTION

The influence of Mg-Fe^{2+} composition on intracrystalline cation distribution was modeled within the framework of the general thermodynamic model for binary solid solutions between spinel end-members described by O'Neill and Navrotsky (1984). In its simplest formulation, cation distribution at equilibrium corresponds to the minimum of free energy of disordering (ΔG_D) with respect to inversion i, i.e., $(\delta \Delta G_D/\delta i)_T = 0$. The change in enthalpy of cation disordering (ΔH_D), relative to the same spinel with normal cation distribution, is shown to vary with $\alpha_{A-B} i + \beta i^2$, where α_{A-B} is the difference in the "site preference enthalpies" of cations A and B. In many cases, β is taken to be constant for 2–3 spinels at –20 kJ/mol, whereas for both spinel s.s. and hercynite β has been found experimentally to be positive and equal to 13 and 19.7 kJ/mol, respectively (Andreozzi et al. 2000; Harrison et al. 1998). Combining this expression of enthalpy of mixing with the configurational entropy of a given cation distribution (ΔS_C), and considering that $\delta \Delta S_C/\delta i$ is proportional to $\ln[i^2/(1-i)(2-i)]$, the following relation connecting i and T at equilibrium is derived:

$$-RT\ln[i^2/(1-i)(2-i)] = \alpha_{A-B} + 2\beta i \quad (3)$$

The cation distributions observed in our samples were compared with those predicted by the general model by applying Equation 3 to binary solid solution $(Mg_{1-y}Fe^{2+}_y)Al_2O_4$. In the ideal case, the cation distribution scheme may be written as:

Site	T	M	Sum
Mg	(1-y-^{VI}Mg)	^{VI}Mg	1-y
Fe^{2+}	(y-$^{VI}Fe^{2+}$)	$^{VI}Fe^{2+}$	y
Al	($^{VI}Fe^{2+}$ + ^{VI}Mg)	(2-$^{VI}Fe^{2+}$-^{VI}Mg)	2
Sum	1	2	3

and the following equations may be derived:

$$-RT\ln[{}^{VI}Fe^{2+}({}^{VI}Fe^{2+} + {}^{VI}Mg)/(y - {}^{VI}Fe^{2+})(2 - {}^{VI}Fe^{2+} - {}^{VI}Mg)] = \alpha_{Fe-Al} + 2\beta_{Fe-Al}{}^{VI}Fe^{2+} + (\beta_{Fe-Al} + \beta_{Mg-Al})^{VI}Mg \quad (4)$$

$$-RT\ln[{}^{VI}Mg({}^{VI}Fe^{2+} + {}^{VI}Mg)/(1 - y - {}^{VI}Mg)(2 - {}^{VI}Fe^{2+} - {}^{VI}Mg)] = \alpha_{Mg-Al} + 2\beta_{Mg-Al}{}^{VI}Mg + (\beta_{Fe-Al} + \beta_{Mg-Al})^{VI}Fe^{2+} \quad (5)$$

where T = 1073 K, α_{Fe-Al} = 31.3 kJ/mol and β_{Fe-Al} = 19.7 kJ/mol (Harrison et al. 1998) and α_{Mg-Al} = 23 kJ/mol and β_{Mg-Al} = 13 kJ/mol (Andreozzi et al. 2000). Numerical solutions of equations (4) and (5) were found, and the calculated values of $^{VI}Fe^{2+}$ and ^{VI}Mg are reported in Table 5.

The agreement between experimental and calculated inversion data is quite satisfactory (Fig. 3). Minor symmetrical deviations may be observed in the middle of the series, where calculated $^{VI}Fe^{2+}$ and ^{VI}Mg are slightly over- and under-estimated, respectively. However, this deviation becomes nil at the hercynite end-member, which means that there is no systematic effect due to the low Fe^{3+} content of the samples.

INFLUENCE OF COMPOSITION ON Fe^{2+}-Mg INTERSITE DISTRIBUTION AND GEOTHERMOMETRIC IMPLICATIONS

The spinel crystals studied here underwent the same thermal history, and the equilibration temperature is about 800 °C for all samples. Therefore, the inversion trend observed from spinel s.s. to hercynite must be related to compositional variations.

The relation between inversion (i) and bulk composition (y) may be expressed by $^{IV}Mg/(1-i) = (1-y)$ and $^{IV}Fe^{2+}/(1-i) = y$ (Fig. 4). It follows that, at constant temperature, Fe-Mg ordering is influenced not only by bulk composition and overall degree of inversion, but also by the tetrahedral preference of Fe^{2+} with respect to Mg. To account for this last effect, an-

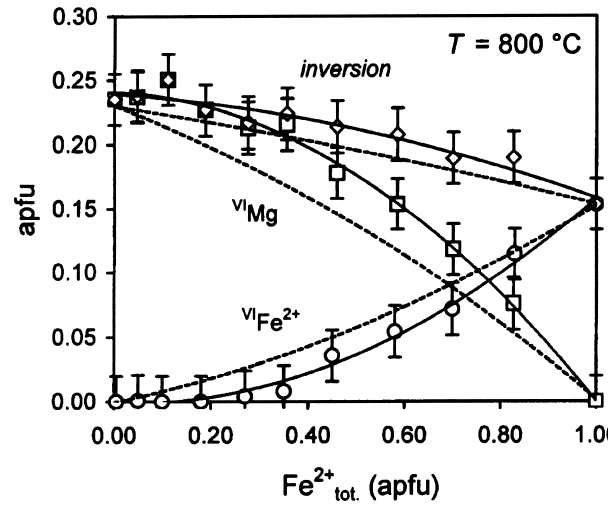

FIGURE 3. Variations in Fe-Mg distribution and inversion (i) in spinel s.s.-hercynite synthetic samples as a function of hercynite content. Solid lines = best fit to experimental data; error bars = ±2σ. Dashed lines = calculated values using model of O'Neill and Navrotsky (1984).

TABLE 5. Synthetic crystals belonging to spinel s.s. - hercynite series: Fe^{2+}-Mg distributions and inversion values calculated from O'Neill and Navrotsky thermodynamic model compared with those obtained from experimental data

Sample	SP3/10a	He2f/e	He3a/b	He4a/c	He4b/d	He5a/a	He6a/e	He7a/b	He8a/h	He9a/h	He100c/a
$^{VI}Fe^{2+}_{calc.}$	0.000	0.000	0.009	0.018	0.028	0.038	0.052	0.070	0.090	0.114	0.154
$^{VI}Mg_{calc.}$	0.230	0.225	0.214	0.200	0.184	0.168	0.147	0.119	0.090	0.055	0.000
$i_{calc.}$	0.230	0.225	0.223	0.218	0.212	0.206	0.198	0.189	0.180	0.169	0.154
$^{VI}Fe^{2+}_{exp.}$	–	0.00(1)	0.00(1)	0.00(1)	0.00(1)	0.01(1)	0.04(1)	0.05(1)	0.07(1)	0.11(1)	0.15(1)
$^{VI}Mg_{exp.}$	0.24(1)	0.24(1)	0.25(1)	0.23(1)	0.21(1)	0.21(1)	0.18(1)	0.15(1)	0.12(1)	0.08(1)	–
$i_{exp.}$	0.24(1)	0.24(1)	0.25(1)	0.23(1)	0.21(1)	0.22(1)	0.22(1)	0.20(1)	0.19(1)	0.19(1)	0.15(1)

Notes: All values in atoms per formula unit. Experimental data estimated standard deviation (±1σ) in brackets.

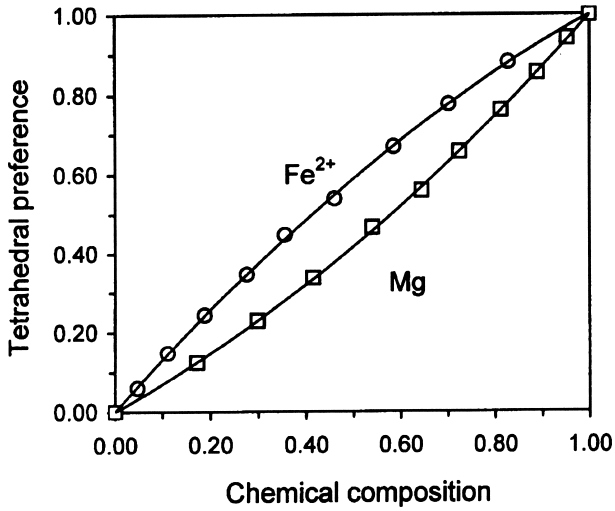

FIGURE 4. Tetrahedral site preference of Fe^{2+} and Mg in spinel s.s.-hercynite synthetic samples, expressed as $^{IV}Fe^{2+}/(1 - i)$ vs. $Fe^{2+}_{tot.}$ and $^{IV}Mg/(1 - i)$ vs. Mg_{tot}. Solid line = best fit to experimental data.

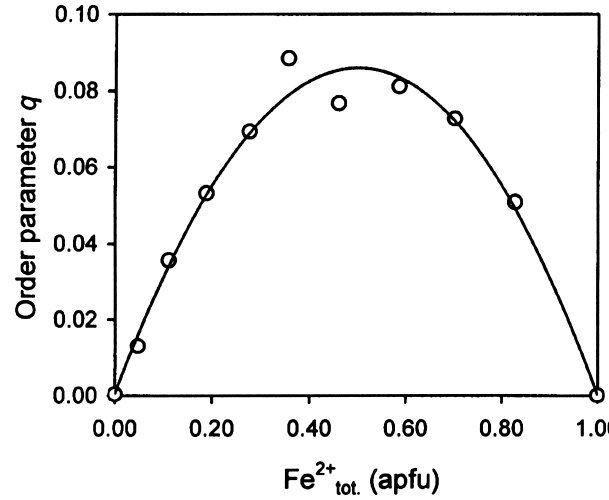

FIGURE 5. Variations in order parameter q with hercynite content in spinel s.s.-hercynite samples. Solid line = best fit to experimental data. Variations in q show symmetrical positive deviation from Fe^{2+}-Mg ideal mixing ($q = 0$) and define preference of Fe^{2+} for tetrahedral site.

other order parameter (q), which is independent of the overall degree of inversion and defines the tetrahedral site preference of Fe^{2+} with respect to Mg, must be introduced. The tetrahedral cation distribution is then:

$$^{IV}Mg = (1 - y - q)(1 - i) \quad (6)$$

$$^{IV}Fe^{2+} = (y + q)(1 - i). \quad (7)$$

A value of $q = 0$ refers to ideal mixing of Mg and Fe^{2+} regardless of the particular degree of inversion, positive q values define the preference of Fe^{2+} for the tetrahedral site, and negative ones an octahedral preference. It is noteworthy that, in the spinel s.s.-hercynite series, any variation in q as a function of bulk composition shows a symmetrical positive deviation from ideality (Fig. 5).

From an energy point of view, the observed inversion trend is a clear indication that, for a given temperature, the intersite exchange Mg ↔ Al is favored with respect to Fe^{2+} ↔ Al.

Inspection of literature data shows that relationships between Fe^{2+}-Mg intracrystalline distribution and hercynite content are not straightforward. Our results show that the percentage of octahedral Fe^{2+} with respect to total Fe^{2+} content, $^{VI}Fe^{2+}/Fe^{2+}_{tot.}$, increases from zero to 15% as a function of hercynite content (Fig. 6). In particular, the $^{VI}Fe^{2+}/Fe^{2+}_{tot.}$ ratio markedly rises in the hercynite-rich part of the series—that is, where Mg content is lower than Fe^{2+}—and this is in line with the tetrahedral preference of Fe^{2+}. Instead, the trend derived from the data of Larsson (1994, 1995) and Larsson et al. (1994) suggests almost constant disorder for Fe^{2+}, around 20% of $Fe^{2+}_{tot.}$ all along the spinel s.s.-hercynite join. Although $^{VI}Fe^{2+}/Fe^{2+}_{tot.}$ ratios suffer from large uncertainties, especially at low hercynite content, this trend does not fit either our data or the predictions of the O'Neill and Navrotsky model.

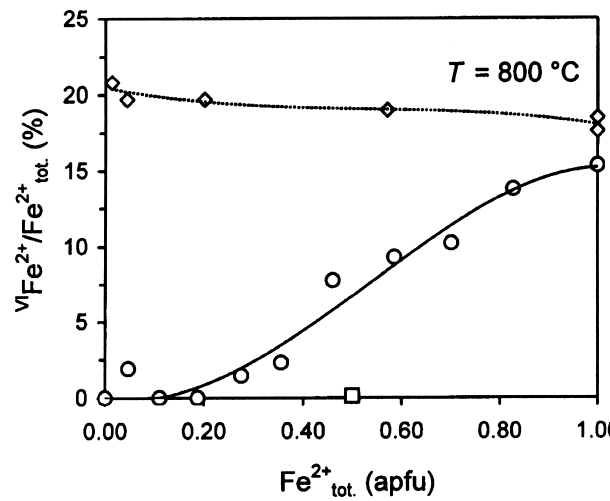

FIGURE 6. Variations in $^{VI}Fe^{2+}/Fe^{2+}_{tot.}$ ratio as a function of hercynite content in spinel s.s.-hercynite samples. Circles = this study, interpolated by solid line; diamonds = data from Larsson (1994, 1995) and Larsson et al. (1994), interpolated by dotted line; square = sample from Nozik and Kocharov (1989).

The definition of the actual trend followed by Fe^{2+}-Mg ordering as a function of both composition and temperature has important geothermometric implications, because Fe^{2+}-bearing spinels are common in nature and may be used to reconstruct the cooling history of host-rocks. Most natural spinels are characterized by hercynite contents far lower than 50%, and the trend outlined by our samples accounts for the very low amount of Fe^{2+} disorder ($^{VI}Fe^{2+}/Fe^{2+}_{tot.}$ always lower than 10%) commonly reported in the literature (Della Giusta et al. 1996; Lucchesi and Della Giusta 1997; Lucchesi et al. 1998a).

ACKNOWLEDGMENTS

The authors gratefully acknowledge H. Skogby and the Mineralogy Department of the National Museum for Natural History, Stockholm, for precious collaboration during crystal synthesis, R. Carampin, CNR, Padova, for assistance during the microprobe stage, and G. Walton for revision of the English manuscript. F. Bosi and F. Garramone assisted during X-ray data collection, F. Bosi collaborated in the solution of the equations of the thermodynamic model. A.M. Conte is thanked for her invaluable support during manuscript development. Critical review by Prof. Della Giusta, University of Padova and of two anonymous referees greatly improved the manuscript, particularly the thermodynamic modeling section. This work was funded by CNR and MURST grants and carried out within scientific programs and with the financial support of the C.S.-CNR "Equilibri sperimentali in minerali e rocce."

REFERENCES CITED

Andreozzi, G.B. (1999) Synthetic spinels in the (Mg,Fe^{2+},Zn)(Al,Fe^{3+})$_2O_4$ system: I. Flux growth of single crystals. Periodico di Mineralogia, 68, 43–51.

Andreozzi, G.B., Princivalle, F., Skogby, H., and Della Giusta, A. (2000) Cation ordering and structural variations with temperature in $MgAl_2O_4$ spinel: an X-ray single crystal study. American Mineralogist, 85, 1164–1171.

Andreozzi, G.B., Lucchesi, S., Skogby, H., and Della Giusta, A. (2001) Compositional dependence of cation distribution in some synthetic (Mg,Zn)(Al,Fe^{3+})$_2O_4$ spinels. European Journal of Mineralogy, 13, 391–402.

Basso, R., Comin-Chiaromonti, P., Della Giusta, A., and Flora, O. (1984) Crystal chemistry of four Mg-Fe-Al-Cr spinels from the Balmuccia peridotite (Western Italian Alps). Neues Jahrbuch für Mineralogie Abhandlungen, 150, 1–10.

Bohlen, S.R., Dollase, W.A., and Wall, V.J. (1986) Calibration and applications of spinel equilibria in the system FeO-Al_2O_3-SiO_2. Journal of Petrology, 27, 1143–1156.

Carbonin, S., Russo, U., and Della Giusta, A. (1996) Cation distribution in some natural spinels from X-ray diffraction and Mössbauer spectroscopy. Mineralogical Magazine, 60, 355–368.

Cremer, V. (1969) Die Mischkristallbildung im System Chromit-Magnetit-Hercynit zwischen 1000° und 500° C. Neues Jahrbuch für Mineralogie Abhandlungen, 111, 184–205.

Della Giusta, A., Carbonin, S., and Ottonello, G. (1996) Temperature-dependent disorder in a natural Mg-Al-Fe^{2+}-Fe^{3+}-spinel. Mineralogical Magazine, 60, 603–616.

Hafner, S. (1960) Metalloxyde mit Spinellstruktur. Schweizerische Mineralogische und Petrographische Mitteilungen, 40, 208–240.

Hålenius, U., Skogby, H., and Andreozzi, G.B. (2002) Influence of cation distribution on the optical absorption spectra of Fe^{3+}-bearing spinel s.s. –hercynite crystals: evidence for electron transitions in $^{VI}Fe^{2+}$-$^{VI}Fe^{3+}$ clusters. Physics and Chemistry of Minerals, in press.

Harrison, R.J., Redfern, S.A.T., and O'Neill, H.St.C. (1998) The temperature dependence of the cation distribution in synthetic hercynite ($FeAl_2O_4$) from in-situ neutron diffraction refinements. American Mineralogist, 83, 1092–1099.

Hill, R.J. (1984) X-ray powder diffraction profile refinement of synthetic hercynite. American Mineralogist, 69, 937–942.

Hill, R.J., Craig, J.R., and Gibbs, G.V. (1979) Systematics of the spinel structure type. Physics and Chemistry of Minerals, 4, 317–340.

Kristiansson, P., Hålenius, U., Skogby, H., Elfman, M., Malmqvist, K., and Pallon, J. (1999) Boron distribution in single crystals investigated by nuclear reaction analysis. Nuclear Instruments and Methods in Physics Research, B 158, 562–567.

Larsson, L. (1994) Temperature dependence of the intra-crystalline distribution in some iron-containing spinels. Ph.D. thesis, Acta Universitatis Upsaliensis, Uppsala, 1994.

———(1995) Temperature-dependent cation distribution in a natural $Mg_{0.4}Fe_{0.6}Al_2O_4$ spinel. Neues Jahrbuch für Mineralogie Monatshefte, 173–184.

Larsson, L., O'Neill, H.St.C., and Annersten, H. (1994) Crystal chemistry of synthetic hercynite ($FeAl_2O_4$) from XRD structural refinements and Mössbauer spectroscopy. European Journal of Mineralogy, 6, 39–51.

Lavina, B., Salviulo, G., and Della Giusta, A. (2002) Cation distribution and structure modeling of spinel solid solutions. Physics and Chemistry of Minerals, 29, 10–18.

Lehmann, J. and Roux, J. (1986) Experimental and theoretical study of (Fe^{2+},Mg)(Al,Fe^{3+})$_2O_4$ spinels: activity-composition relationships, miscibility gaps, vacancy contents. Geochimica et Cosmochimica Acta, 50, 1765–1783.

Lucchesi, S. and Della Giusta, A. (1997) Crystal chemistry of a highly disordered Mg-Al natural spinel. Mineralogy and Petrology, 59, 91–99.

Lucchesi, S., Russo, U., and Della Giusta, A. (1997) Crystal chemistry and cation distribution in some Mn-rich natural and synthetic spinels. European Journal of Mineralogy, 9, 31–42.

Lucchesi, S., Amoriello, M., and Della Giusta, A. (1998a) Crystal chemistry of spinels from xenoliths of the Alban Hills volcanic region. European Journal of Mineralogy, 10, 473–482.

Lucchesi, S., Della Giusta, A., and Russo, U. (1998b) Cation distribution in natural Zn-aluminate spinels. Mineralogical Magazine, 62, 41–54.

Lucchesi, S., Russo, U., and Della Giusta, A. (1999) Cation distribution in natural Zn-spinels: franklinite. European Journal of Mineralogy, 11, 501–511.

Mason, T.O. and Bowen, H.K. (1981) Cation distribution and defect chemistry of iron-aluminate spinels. Journal of the American Ceramic Society, 64, 86–90.

Nozik, Yu. Z. and Kocharov, A.G. (1989) Neutron-diffraction study of the distribution of cations in the spinel $Fe_{0.5}Mg_{0.5}Al_2O_4$. Kristallografiya, 34, 616–617.

Okaj, T., Wada, H., and Fujinuki, T. (1996) Ignition and chemical resistance tests of platinum and platinum-alloy crucibles for chemical analysis. Bunseki-Kagaku, 45, 1127–1132.

O'Neill, H.St.C. and Navrotsky, A. (1983) Simple spinels: crystallographic parameters, cation radii, lattice energies and cation distributions. American Mineralogist, 68, 181–194.

———(1984) Cation distribution and thermodynamic properties of binary spinel solid solutions. American Mineralogist, 69, 733–753.

Pouchou, J.L. and Pichoir, F. (1984) A new model for quantitative X-ray microanalysis. I. Application to the analysis of homogeneous samples. La Recherche Aérospatiale, 3, 13–36.

Princivalle, F., Della Giusta, A., and Carbonin, S. (1989) Comparative crystal chemistry of spinels from some suites of ultramafic rocks. Mineralogy and Petrology, 40, 117–126.

Princivalle, F., Della Giusta, A., De Min, A., and Piccirillo, E.M. (1999) Crystal chemistry and significance of cation ordering in Mg-Al rich spinels from high-grade hornfels (Predazzo-Monzoni, NE Italy). Mineralogical Magazine, 63, 257–262.

Redfern, S.A.T., Harrison, R.J., O'Neill, H.St.C., and Wood, D.R.R. (1999) Thermodynamics and kinetics of cation ordering in $MgAl_2O_4$ spinel up to 1600°C from in situ neutron diffraction. American Mineralogist, 84, 299–310.

Roth, W.L. (1964) Magnetic properties of normal spinels with only A-A interactions. Le Journal de Physique, 25, 507–515.

Slack, G.A. (1964) $FeAl_2O_4$-$MgAl_2O_4$: Growth and some thermal, optical, and magnetic properties of mixed single crystals. Physical Review, 134, A1268–A1280.

Tokonami, M. and Horiuchi, H. (1980) On the space group of spinel $MgAl_2O_4$. Acta Crystallographica, A36, 122–126.

Turnock, A. and Eugster, H.P. (1962) Fe-Al Oxides: phase relationships below 1,000°C. Journal of Petrology, 3, 533–565.

Waerenborgh, J.C., Figueiredo, M.O., Cabral, J.M.P., and Pereira, L.C.J. (1994a) Powder XRD structure refinements and ^{57}Fe Mössbauer effect study of synthetic $Zn_{1-x}Fe_xAl_2O_4$ ($0 < x \leq 1$) spinels annealed at different temperatures. Physics and Chemistry of Minerals, 21, 460–468.

———(1994b) Temperature and composition dependence of the cation distribution in synthetic $ZnFe_yAl_{2-y}O_4$ ($0 \leq y \leq 1$) spinels. Journal of Solid State Chemistry, 111, 300–309.

Zhukovskaya, T.N., Camokhvalova, O.L., Bushueva, E.V., and Chichagov, A.V. (1980) Hydrothermal synthesis and study of some physical properties of spinels in the composition $Mg_{1-x}Fe_xAl_2O_4$. Zapiski Vsesoyuznogo Mineralogicheskogo Obshchestva, 109, 367–369 (in Russian).

MANUSCRIPT RECEIVED JUNE 5, 2001
MANUSCRIPT ACCEPTED MARCH 12, 2002
MANUSCRIPT HANDLED BY PETER C. BURNS